



HAL
open science

Behavior and Fate of Halloysite Nanotubes (HNTs) When Incinerating PA6/HNTs Nanocomposite

Ghania Ounoughene, Olivier Le Bihan, C. Chivas-Joly, C. Motzkus, C. Longuet, Bruno Debray, Aurélie Joubert, Laurence Le Coq, José-Marie Lopez-Cuesta

► **To cite this version:**

Ghania Ounoughene, Olivier Le Bihan, C. Chivas-Joly, C. Motzkus, C. Longuet, et al.. Behavior and Fate of Halloysite Nanotubes (HNTs) When Incinerating PA6/HNTs Nanocomposite. *Environmental Science and Technology*, 2015, 49 (9), pp.5450-5457. 10.1021/es505674j . hal-01201688

HAL Id: hal-01201688

<https://imt-atlantique.hal.science/hal-01201688>

Submitted on 30 Aug 2019

HAL is a multi-disciplinary open access archive for the deposit and dissemination of scientific research documents, whether they are published or not. The documents may come from teaching and research institutions in France or abroad, or from public or private research centers.

L'archive ouverte pluridisciplinaire **HAL**, est destinée au dépôt et à la diffusion de documents scientifiques de niveau recherche, publiés ou non, émanant des établissements d'enseignement et de recherche français ou étrangers, des laboratoires publics ou privés.

Behavior and Fate of Halloysite Nanotubes (HNTs) When Incinerating PA6/HNTs Nanocomposite

G. Ounoughene,^{†,‡,§} O. Le Bihan,^{*,||} C. Chivas-Joly,[⊥] C. Motzkus,[⊥] C. Longuet,[‡] B. Debray,^{||} A. Joubert,[†] L. Le Coq,[†] and J.-M. Lopez-Cuesta^{*,‡}

[†]LUNAM, Ecole des Mines de Nantes, GEPEA, CNRS, UMR 6144, 4 rue Alfred Kastler, 44307 Nantes Cedex 03, France

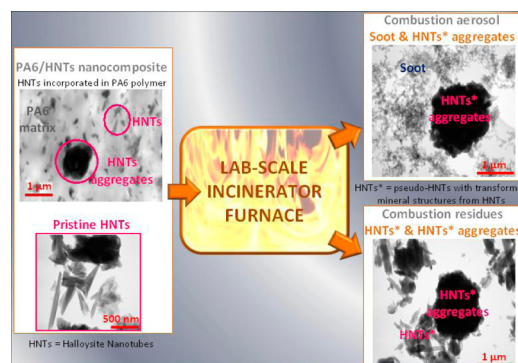
[‡]C2MA, Ecole des Mines d'Alès, 6 Avenue de Clavières, 30319 Alès Cedex, France

[§]ADEME, 20 avenue du Grésillé, 49004 Angers Cedex 01, France

^{||}INERIS, Parc Technologique Alata, 60550 Verneuil-en-Halatte, France

[⊥]LNE, 29 Avenue Roger Hennequin, 78197 Trappes Cedex, France

ABSTRACT: Nanoclay-based nanocomposites have been widely studied and produced since the late 1990s, and frequently end up in waste disposal plants. This work investigates the behavior of PA6/HNTs nanocomposites (nylon-6 incorporating halloysite nanotubes) during incineration. Incineration tests were performed at lab-scale using a specific tubular furnace modified in order to control the key incineration parameters within both the combustion and postcombustion zones. The combustion residues and combustion aerosol (particulate matter and gas phase) collected downstream of the incinerator furnace were characterized using various aerosol analysis techniques. Time tracking of the gas and particle-number concentrations revealed two-step char formation during combustion. HNTs transformed into other mineral structures which were found in both the aerosol and the residues. During combustion of the polymer, it appears that HNTs contribute to the formation of a cohesive char layer that protects the residual material.



2. INTRODUCTION

25 In recent decades, polymer nanocomposites have drawn much
26 attention due to their enhanced performance.^{1–4} The physico-
27 chemical properties of polymer matrices (tensile strength,
28 stiffness, heat resistance, barrier properties, etc.) are enhanced
29 by adding small amounts of nano-objects. This is the case with
30 polyamide 6 (PA6) incorporating silicate nanoclays. These
31 nanocomposites have been extensively studied and developed by
32 both universities and industry for many applications in various
33 industrial areas such as transportation, electronic and electrical
34 equipment, and packaging. Nevertheless, many of these state-of-
35 the-art materials are expected to end up in waste treatment
36 facilities such as incineration plants due to the lack of specific
37 recovery procedures.⁵ Hence, the potential environmental risk
38 arising from the incineration of waste containing nanomaterials
39 is a new field which deserves further attention. Some recent
40 studies have begun to focus on this topic, but the data are
41 incomplete.^{5–12} The present study therefore gives some insight
42 into the fate and behavior of nano-objects (incorporated in a
43 polymer matrix) during the incineration of nanocomposites. The
44 work focuses on PA6/HNTs nanocomposites (nylon-6 incor-
45 porating halloysite nanotubes).

46 Polyamide 6 (also called Nylon-6) is a semicrystalline
47 polyamide thermoplastic used in a wide range of fiber, film and
48 engineering applications. It has been shown that a small amount

(1–10 wt %) of silicate nanofiller can remarkably enhance the
properties of the material.^{2,13} Nanofillers based on montmor-
illonite layered silicates have been the subject of many studies.
More recently, halloysite nanotubes (HNTs) have also been
studied, and have been reported to improve many properties,
especially thermal properties, when incorporated in a PA6
polymer matrix.^{14–17} HNTs are aluminosilicates. Their
chemical composition is $\text{Al}_2\text{Si}_2\text{O}_5(\text{OH})_4 \cdot 2\text{H}_2\text{O}$. They are
extracted from natural deposits and are chemically similar to
kaolinite. Their nanotubular structure gives them very interesting
properties that attract the attention of researchers for many
applications.^{17–19}

Many articles and book chapters have been published about
the thermal degradation of nanocomposites,^{13,16,20–25} but none
of them relate to tests involving the combustion parameters of
incineration (temperature around 850 °C, highly ventilated
combustion, at least 2 s residence time for the combustion gas in
a postcombustion chamber at 850 °C, and high oxygen/fuel
contact) or time tracking of the gas and particle concentrations
in the combustion aerosol. In the present work, we used a

69 laboratory scale furnace modified to control the key incineration
 70 parameters. The combustion aerosol was sampled downstream
 71 of the postcombustion chamber (i.e., analogous to upstream of
 72 filtration in a real-scale incineration plant), and was characterized
 73 using various aerosol analysis techniques. This was a first step in
 74 the evaluation of the efficiency of flue-gas cleaning systems. After
 75 that, the combustion residues were analyzed. The aim of this
 76 work is to study the behavior and the fate of HNTs during
 77 incineration of PA6/HNTs nanocomposites while investigating
 78 the influence of HNTs on combustion mechanisms (aerosol
 79 release and decomposition) and the release of nano-objects
 80 during incineration. It is relevant to ask whether the nano-objects
 81 initially incorporated in the polymer are destroyed or undergo
 82 changes during their stay in the incinerator and their fate
 83 thereafter.

3. MATERIALS AND METHODS

84 **3.1. Sample Preparation and Characterization.** PA6/
 85 HNTs nanocomposites (see Supporting Information (SI),
 86 Table S1) were prepared by melt extrusion and injection
 87 molding. The halloysite (shown in Figure 1) was provided by

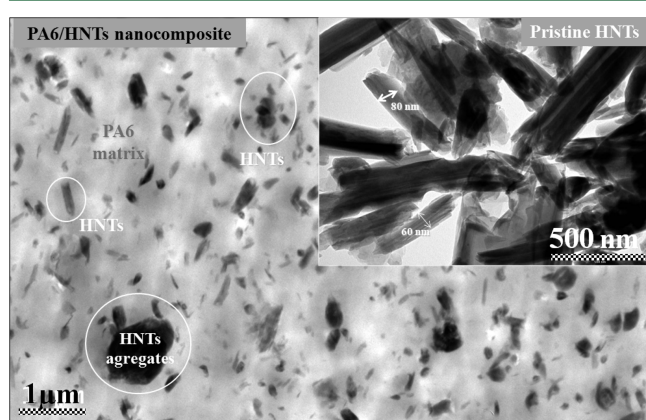


Figure 1. Pristine HNTs dispersed in PA6/HNTs nanocomposite.

88 Imerys Ceramics from New Zealand. PA6 (polyamide 6)
 89 Technyl C206 was supplied by Rhodia Plastics Engineering
 90 SA. Neat matrix and two nanocomposites at two loadings (1 and
 91 5%wt) of HNTs were prepared using the same extrusion and
 92 injection process to ensure the same thermo-chemical history for

all samples. A twin-screw extruder (Clextral BC21, 1200 mm
 length) was used (rotational speed of 250 rpm, and processing
 temperature of 260 °C). The pelletized extruded material
 obtained was finally injection molded (Krauss Maffei KM50/
 180CX) into standard specimens (100 × 100 × 4 mm³). 250 mg
 samples from these specimens were cut and then tested in the
 incinerator furnace.

The pristine HNTs and the prepared nanocomposite samples
 were characterized prior to the incineration tests. Imagery on
 pristine HNTs and on the dispersion of HNTs in the nano-
 composite (Figure 1) was carried out using transmission elec-
 tronic microscope (Philips CM12 TEM 200 kV). In addition,
 elemental analysis of the polymer material, laser diffraction and
 X-ray fluorescence analysis of pristine Halloysite were performed
 (see SI, Tables S2 and S3 and Figure S2). TEM micrographs
 show the nanotubular structure of the pristine halloysite (Figure 1).
 In agreement with literature,^{14–18} the observed halloysite tubes
 are nanosized with a thickness lower than 100 nm.

Thermogravimetric analysis (TGA) was performed using a
 Pyris-1 Perkin–Elmer apparatus. Samples of 10 (±2) mg were
 heated under a nitrogen flow at a 10 °C/min heating rate from
 ambient temperature to 850 °C.

PCFC (pyrolysis combustion flow calorimeter) tests were
 carried out using a fire testing technology apparatus (FTT,
 ASTM D7309). A sample of 2 (±1) mg was heated under
 nitrogen flow to 750 °C at a heating rate equal to 1 K/s. Gases
 were extracted and sent to a combustion chamber in the presence
 of a N₂/O₂ flow (80/20). The combustor ensured complete oxida-
 tion of pyrolysis products at a combustion temperature fixed at
 900 °C.²⁶

3.2. Lab-Scale Incinerator and Analysis. Laboratory scale
 incineration tests were performed using a specific tubular
 furnace. The combustion conditions implemented in the lab-
 scale incinerator furnace (within both the combustion and
 postcombustion zones) were controlled to satisfy the key
 operational parameters that govern an incineration process,
 that is, chiefly temperature (850 °C in the combustion and
 postcombustion-zone), residence time (at least two seconds in
 the postcombustion zone at 850 °C), air-excess (never below
 11% of oxygen) and turbulence (a good mix between
 combustible and oxygen). A tubular horizontal furnace
 (Carbolite STF 15/610 Horizontal Tube Furnace) was modified
 to obtain as close as possible to the combustion conditions
 implemented in an industrial grate incinerator. As illustrated in

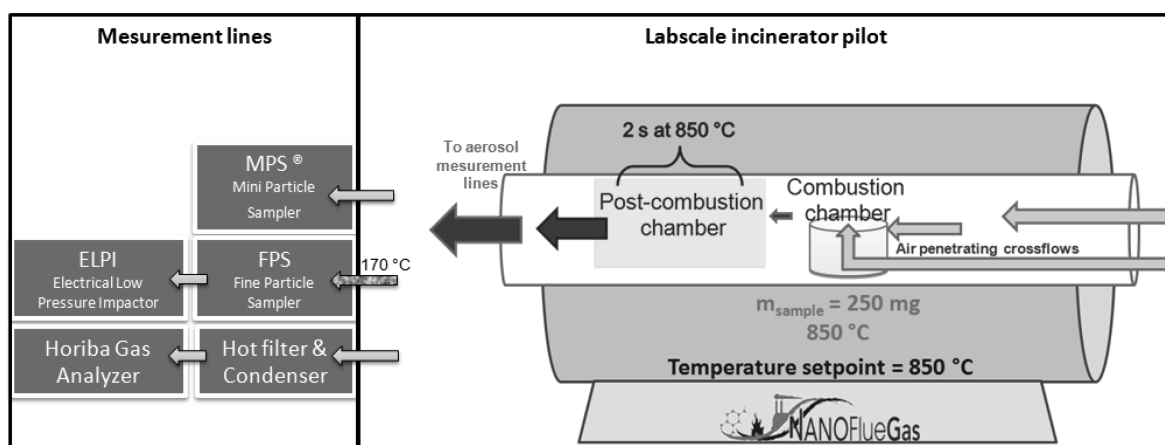


Figure 2. Basic diagram of the modified tubular furnace—Lab-scale incinerator and the measurement lines.

137 Figure 2 the “combustion chamber” is maintained at 850 °C
138 (at least) and where air cross flows penetrate and mix with the
139 combustibles. Then, the “post-combustion chamber” is the
140 furnace zone where the combustion aerosol stays 2 s at 850 °C
141 (at least).

142 Finally the combustion released gases and the aerosol particles
143 were conveyed to the measurement line as described in the
144 following paragraph.

145 In order to superimpose the curves of time tracking, it is
146 important to know the response time of each measurement
147 line to synchronize all events detected. The reaction time of each
148 unit of the measurement line is determined by stopwatch. An
149 uncertainty of two seconds is taken into account.

150 The combustion aerosol was sampled appropriately as
151 explained below and analyzed in three different ways: time
152 tracking for the gas and particles from the aerosol and two off-line
153 analyses for the particulate matter. Further analyses were
154 conducted on the combustion residues.

155 **3.2.1. Time Tracking for the Gas Phase.** The sampling of the
156 gas phase from the combustion aerosol followed the methods
157 used for sampling direct emissions from stationary combustion
158 sources. The flue gas leaving the furnace was dried and filtered
159 using a line with a hot filter and a condenser. A multigas analyzer
160 (portable gas analyzer PG-250 Horiba) was used. It indicates
161 the evolution of the combustion gases concentrations: the
162 consumption of O₂ (%_{vol.}) and the production of NO_x (ppm_{vol.}),
163 CO₂ (%_{vol.}) and CO (ppm_{vol.}). They are respectively detected by
164 paramagnetism, chemiluminescence and an infrared technique
165 with 1 s time resolution.

166 **3.2.2. Time Tracking and off-Line Analysis for Particulate
167 Matter.** The combustion aerosol sampled downstream of the
168 postcombustion chamber has to be representative of the aerosol
169 sampled upstream of the flue-gas cleaning systems. The target
170 temperature is 170 (±10) °C. In fact, under industrial conditions,
171 the aerosol leaves the postcombustion chamber and goes
172 through an upstream filtration processes at a temperature
173 around 150 °C in accordance with BREF Waste Incineration
174 (2006).²⁷ Different samplers and impactors were used to
175 conduct the analyses with respect to the temperature constraint
176 mentioned above.

177 Regarding the time tracking of the particles from the
178 combustion aerosol, an electrical low pressure impactor, Dekati
179 (ELPI) was used downstream of a fine particle sampler dilutor
180 (FPS, Dekati). The objective of the sampling was to avoid cold
181 spots below 170 °C before and during the first dilution. FPS
182 dilutor is well adapted to measurements related to combustion
183 research. This system allows sampling from hot flue gas and
184 provides controlled temperature decrease with minimal
185 losses.^{28–30} The FPS dilutor performs two successive dilutions:
186 the first heated dilution at 170 °C and the second at room tem-
187 perature. The primary dilution air was heated to 170 (±10) °C.
188 Thus, the sampled combustion aerosol underwent two dilutions
189 with a total factor of 1:30. The dilution ratio was given in real
190 time by the FPS software. However, in order to check the
191 displayed FPS value, the dilution ratio was recalculated
192 continuously during the test using a gas analyzer connected to
193 the output the FPS which indicates the concentration of CO and
194 CO₂ after the dilution.³¹

195 The ELPI provided a real-time measurement of particle num-
196 ber concentration through 12 channels from 17 nm to 5 μm.³²
197 The PN_{x-y} are defined as the number concentration of particles
198 counted by the ELPI with mean geometric diameter (Di)
199 between *x* and *y* μm.

Regarding off-line analyses, there were two types of sampling: 200
in the first type, combustion aerosol particles were collected 201
throughout the test; in the second type, combustion aerosol 202
particles were collected over a targeted time range. 203

In the first case, the aerosol combustion underwent just one 204
hot dilution at 170 °C with a porous tube dilutor from VTT 205
laboratory (Valtion Teknillinen Tutkimuskeskus Technical 206
research center of Finland).³³ This diluted hot sample was 207
routed to a gravimetric impactor (DGI, Dekati Gravimetric 208
Impactor) which was heated to the same temperature (170 °C ± 209
10 °C). This PM_{2.5} four-stage impactor resolves particles into 210
four size fractions with 50% collection efficiency for aerodynamic 211
(dp50) cut-points of 2.5, 1.0, 0.5, 0.2 μm plus a back-up filter 212
(after the impaction stages) which collects all particles typically 213
smaller than 0.2 μm.³⁴ In this way, the particulate matter of 214
the combustion aerosol was collected on PTFE impaction 215
substrates with controlled temperature during sampling. Then, 216
these particles were analyzed by a scanning electronic micro- 217
scope (JEOL 7600F High Resolution Analytical SEM energy 218
dispersive spectrometer SDD BRUKER (EDS) X-ray detector). 219
This gravimetric impactor provided a qualitative analysis 220
(imagery and chemistry) of particles collected during the 221
whole combustion test. 222

In the second case, particles from the combustion aerosol were 223
collected on a TEM grid for above 10 s downstream of the tubular 224
furnace with a MPS (Mini-Particle-Sampler, Ecomesure³⁵). A 225
Philips CM12 TEM 200 kV was used for the imagery. 226

3.2.3. Analysis of the Combustion Residues. The combus- 227
tion residues in the sample holder of the lab-scale incinerator 228
were collected after each test. They were analyzed by TEM 229
(Philips CM12 TEM 200 kV), and SEM. X-ray diffraction 230
(XRD) with a Bruker AXS D8 Advance diffractometer using Cu 231
Kα radiation. 232

4. RESULTS

**4.1. Time Tracking of Gas Concentration and Particle 233
Number Concentration.** The graphs showing the evolution of 234
concentrations during the incineration of the nanocomposite 235
PA6/SHNTs are given in Figure 3a. The two verticals delimit 236
the time range with more than 5% O₂ consumption from the 237
baseline. This area of interest is denoted “AOI”. The averages of 238
three runs are presented with the associated standard deviation. 239
When the neat matrix is compared to the nanocomposite, weight 240
standardization was performed in order to compare the same 241
mass of polymer. 242

Before the AOI, from 0 to 48 s, O₂ consumption is low, little 243
gases are produced, but particles are strongly emitted with a 244
domination of PN_{0.1}. Ignition is observed during this period. 245
During the AOI, which extends over a period from 48 to 100 s, 246
oxygen consumption is maximal. From 48 to 80 s, peaks of CO₂, 247
CO and NO_x are noticed while PN_{x-y} decreases. From 80 to 248
100 s, a second peak of CO begins along with an increase in 249
PN_{0.1}. After the AOI, from 100 s to the end (250 s) a shoulder in 250
NO_x concentration appears with a second peak of CO, particles 251
are less and less emitted, and O₂ reaches its baseline. 252

High concentration levels are noticed here. Then, considering 253
such high concentrations, coagulation/agglomeration phenom- 254
ena must occur in the furnace. Even if the pilot does respect a 255
residence time of two seconds, it would be difficult to say if these 256
phenomena occur in a real scale industrial furnace. This is rightly 257
a limit of an incinerator lab-scale pilot. 258

Figure 3b–d show the comparisons between neat PA6 and 259
PA6/SHNTs nanocomposite. A second phase of particle 260

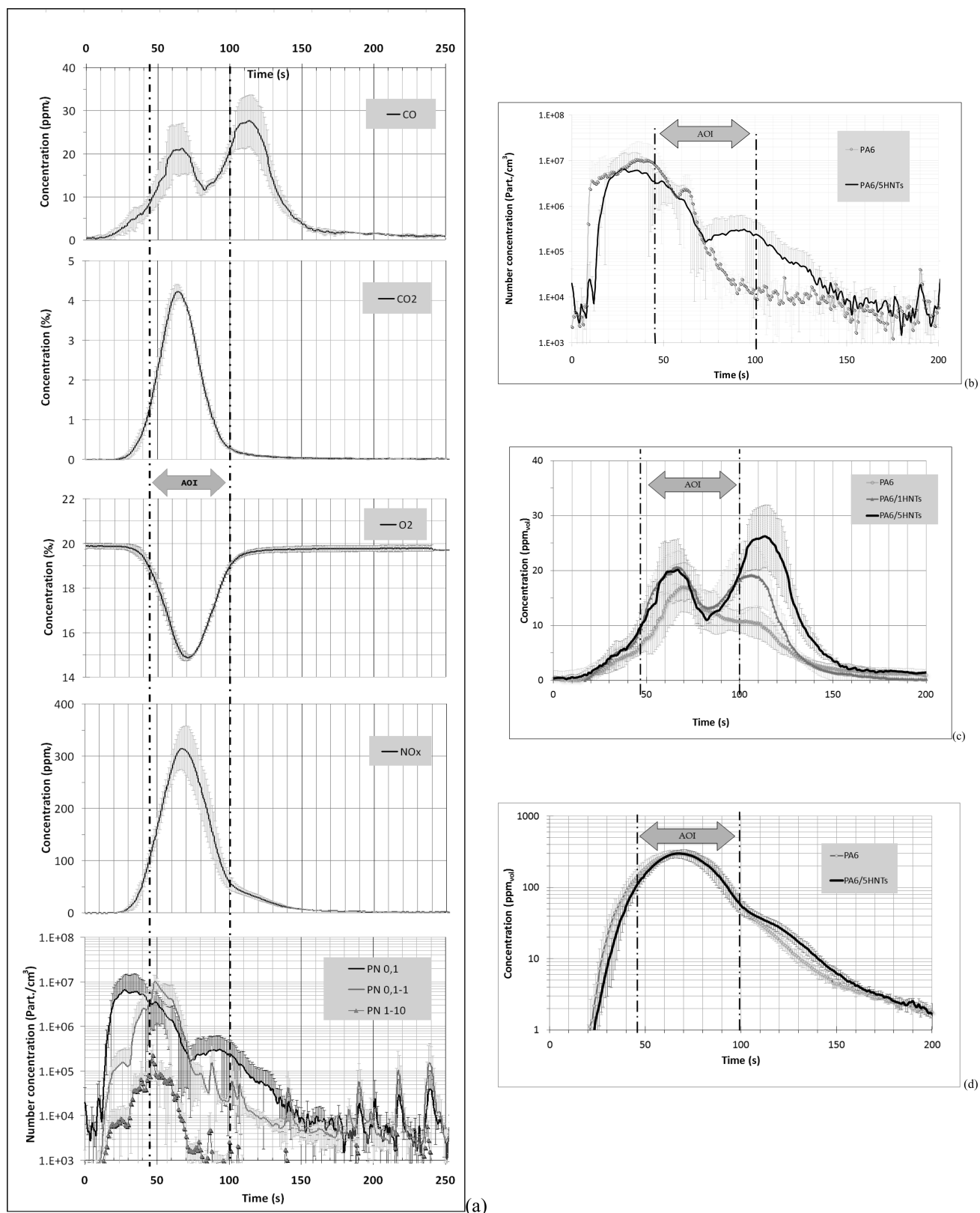


Figure 3. (a) Time tracking for PA6/SHNTs incineration: particle number concentration and gas concentration, (b) Comparison between PA6 and PA6/SHNTs for PN_{0.1} concentration, (c) Comparison between PA6, PA6/SHNTs and PA6/1HNTs for CO concentration, (d) Comparison between PA6 and PA6/SHNTs for NO_x concentration (log scale).

261 emission is clearly observed, as well as a shoulder in NO_x
 262 concentration and a second peak of CO but only for
 263 nanocomposite. This tendency is the same for PA6/1HNTs

(Figure 3c) with its CO curve just inserted between the two other
 CO curves. Other time tracking comparisons show no significant
 differences (see SI, Figures S3 and S4).

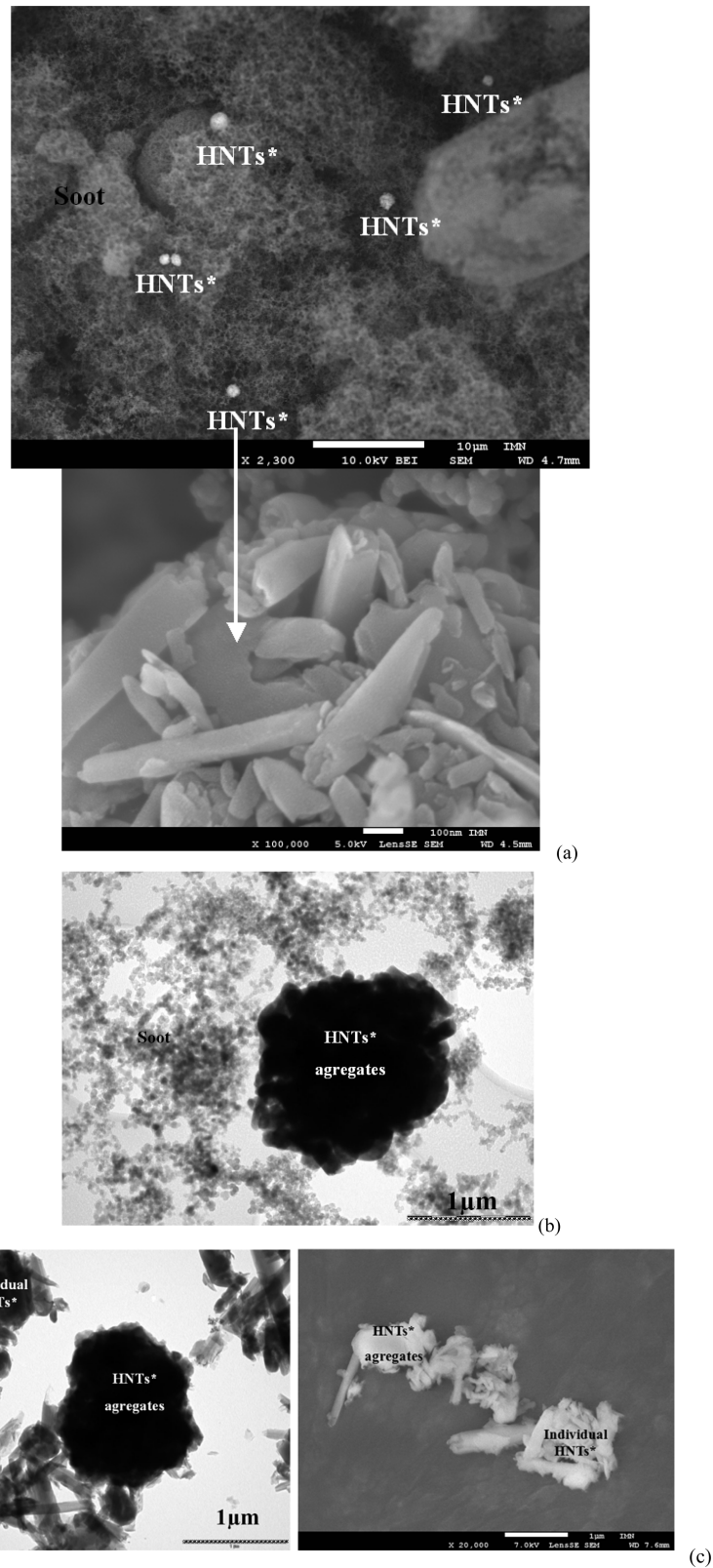


Figure 4. (a) Combustion aerosol particles collected on PTFE impaction substrate: soot and HNTs*, (b) Combustion aerosol particles collected on TEM grid: soot and HNTs* aggregates, (c) Combustion residues: HNTs* aggregates and individual HNTs*.

267 **4.2. Imagery.** The results from imagery provide only
268 qualitative considerations.

269 HNTs* are defined as pseudo-HNTs with transformed
270 mineral structures from HNTs.

271 **4.2.1. Combustion Aerosol Particles.** Imagery on particles
272 collected on PTFE impaction substrates reveals the presence of
273 HNTs* among the soot particles as shown in Figure 4a. These
274 particles are from the fourth stage with $dp50 = 1 \mu\text{m}$. Submicron

275 HNTs* aggregates represent a minor fraction. Figure 4b shows
 276 the particles collected on a TEM grid during ten seconds
 277 preceding AOI. Submicron HNTs* aggregates are also minor
 278 components among the soot particles.

279 **4.2.2. Combustion Residues.** TEM and SEM (coupled with
 280 X-ray microanalysis) performed on combustion residues reveal
 281 that the residues are entirely inorganic and seem to consist of
 282 mineral aggregates and individual mineral particles (Figure 4c).
 283 No residues remain for the neat matrix case since neat PA6
 284 decomposes completely.

285 **4.2.3. TGA and PCFC on Nanocomposite.** Figure 5 presents
 286 TGA curves of neat matrix, pristine HNTs and PA6/SHNTs.

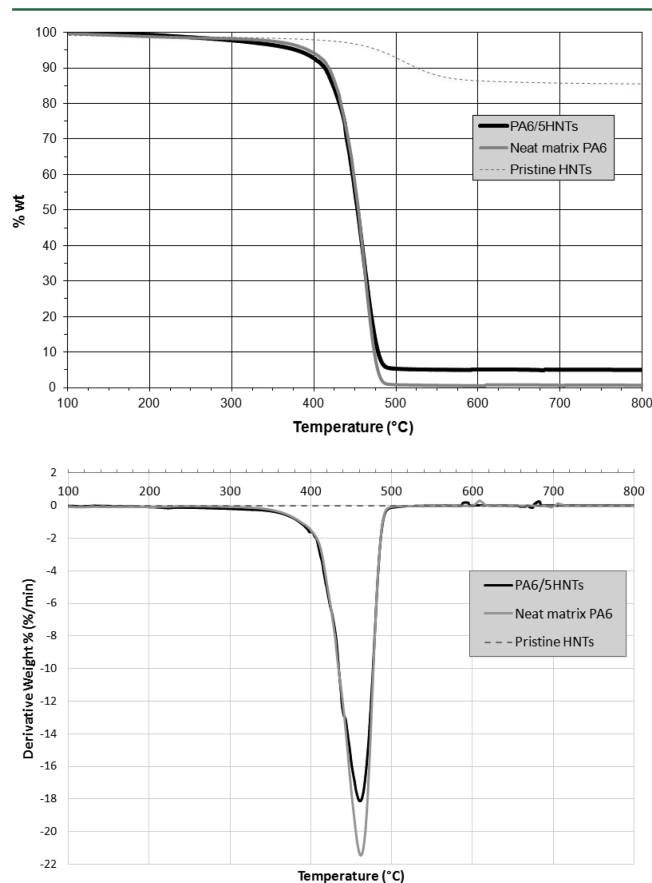


Figure 5. TGA under N₂.

287 The mass loss of HNTs (14%wt) corresponds to water release
 288 and occurs mainly in the 350–600 °C range. The mass loss range
 289 of PA6 occurs between 350 and 500 °C. It can be noticed that the
 290 presence of HNTs reduces the degradation onset temperature
 291 and the thermal stability up to 450 °C.

292 The incorporation of HNTs in PA6 reduces the PCFC peak
 293 (463 W/g for the pristine PA6 and 459 W/g for the composite).
 294 Besides, the shift toward high temperatures is almost un-
 295 noticeable because it is correlated with a mixing law (Figure 5).
 296 Nevertheless, PCFC peaks coincide roughly with the derivatives of
 297 TGA curves (Figure 5, Figure 6). For both techniques, the
 298 thermal degradation of PA6 occurs at lower temperatures in the
 299 presence of HNTs.

300 **4.2.4. XRD on Pristine HNTs and Residues.** For pristine
 301 HNTs, X-ray fluorescence analysis (SI Table S3) and X-ray
 302 diffraction pattern (Figure 7) highlight that quartz (cristobalite)
 303 is present (nodular shape) as impurity of halloysite. The presence

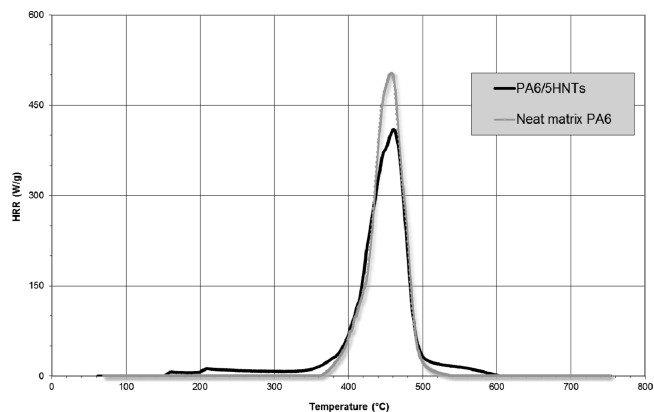


Figure 6. Heat Rate Release at PCFC of neat matrix and PA6/SHNTs nanocomposite.

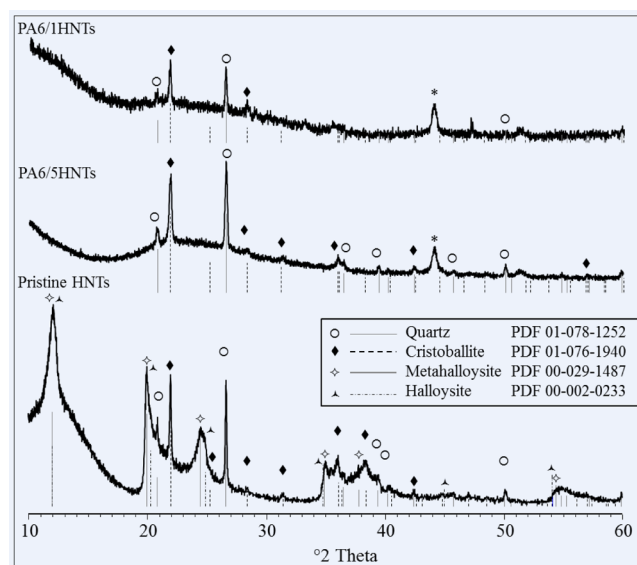


Figure 7. XRD of pristine HNTs and residues of nanocomposites.

of quartz leads to an excess of silicon over aluminum, since in
 pure halloysite, their ratio is 1:1.

XRD spectra performed on residues show that they essentially
 contain cristobalite and quartz. A bump can be noticed for the
 residue from PA6/SHNTs (between $2\theta = 20$ to 30°) which can
 be ascribed to an amorphous aluminosilicate structure. Only a
 peak at 44° was not identified. A temperature of at least 850°C
 is attained in the furnace. Consequently, no halloysite remains
 in the residue even if SEM micrographs show pseudotubular
 structures, also for individual particles.

5. DISCUSSION

Considering the results about time tracking and imagery,
 interpretations can be proposed concerning the behavior and
 fate of HNTs during the incineration of PA6/HNTs nano-
 composites.

5.1. HNTs Behavior: A Two Step Mechanism. First of all,
 a clear difference exists between the neat matrix and the
 nanocomposite. A two-step mechanism can be considered for
 PA6/HNTs nanocomposite. The evidence for this is the second
 CO peak, the NO_x shoulder, and the second phase in the
 emission of particles. Thus, the presence of HNTs is clearly
 responsible for this two step mechanism.

325 It takes around 15 s to introduce the sample in the furnace.
326 This step involves particle emissions due to aerodynamic
327 disturbance from the set up and due to the first thermal effects
328 on the sample. Then, from 15 to 50 s, the thermal decomposition
329 of the sample is indicated by the release of gases and particles, and
330 by the presence of a flame for a few seconds. Effectively, as shown
331 by TGA (Figure 5), HNTs lose water, so a hydrolysis of PA6
332 occurs and there is an increase in the release of volatile
333 combustibles.³⁶ Furthermore, during this step, according to the
334 literature, it is assumed that due to the thermal ablation of the
335 polymer and the dehydration of HNTs, decohesion occurs
336 between the PA6 and the HNTs.^{25,37} Through these processes,
337 the HNTs concentration at the surface of the sample increases
338 and a protective layer gradually forms. TEM observation of
339 particles collected during this phase reveals the presence of
340 HNTs (in small quantities). The high concentration at the
341 surface would promote the release of HNTs and make them free
342 from the matrix and able to be carried away by the aerosol flow.

343 As reported in the literature, polyamide 6 could be considered
344 as a charring polymer and the nanoclays as char promoters.^{24,38}
345 In fact, during a thermal decomposition, some materials can
346 develop on their surface a protective layer which limits mass
347 transfer (volatile combustible and oxygen transfer) as well as
348 thermal transfer. Actually, CO time tracking with a double peak is
349 a good indicator of the protective layer evolution. It was
350 established that the decomposition of charring polymer involve
351 two phases of gas release: the first one is associated with the
352 primary char formation and the second one with the
353 decomposition of the nonstable primary char.^{39,40} Hence in
354 the present case, the protective layer can be made of a
355 carbonaceous char reinforced by HNTs. This char/HNTs layer
356 forms progressively, since under-ventilated combustion occurs
357 with a significant increase in CO emissions (Figure 3c).
358 Simultaneously, the particle emission decreases from 45 s up to
359 70 s (Figure 3a) which is in agreement with the formation of a
360 cohesive char layer. After 65s which corresponds to a CO peak,
361 CO emission decreases and reaches a local minimum while
362 oxygen consumption rises dramatically. This corresponds to the
363 oxidation of the primary char.^{39,40} Moreover, this oxidation is
364 accompanied by an increase in particle emissions, which is
365 irregular and suggests a partial cracking of the protective layer. So
366 the second peak of $PN_{0,1}$ reflects the presence of a second
367 combustion event. Furthermore, the NO_x shoulder from 100 s
368 reflects the oxidation of the residual material which is no longer
369 protected by the cracked char/HNTs layer (Figure 3d).

370 At the end of the combustion test, the residues from PA6/
371 SHNTs incineration consist only of mineral compounds derived
372 from the initial HNTs objects. However, some studies report
373 carbon/clay residues after pyrolysis tests on polymer/clay
374 nanocomposites³⁷ and especially for PA6/HNTs nanocompo-
375 sites.¹⁶ This difference should come from the combustion
376 conditions implemented in the furnace. In fact, in our case the
377 sample is well oxygenated at high temperature (850 °C or more)
378 and for a high rate of increase in temperature (from 25 to 850 °C
379 in 10 s). Therefore, under our incineration conditions, combus-
380 tion is complete and no organic residues remain in the sample
381 holder.

382 As with other nanoclays (montmorillonite for example),
383 HNTs are known to have fire-retardant properties when in-
384 corporated in a polymer matrix.^{16,17} During exposure to a heat
385 source, these refractory materials can protect the matrix in which
386 they are incorporated through the formation of a protective clay
387 barrier which acts as a screen toward mass and heat transfers. The

fire retardancy conferred by HNTs is confirmed by both the 388
reduction in the peak heat release rate (pHRR) observed with the 389
PCFC and the two-step mechanism discussed above. But this 390
retardant character is not effective enough since it has been 391
established that more than 15%wt is necessary to meet fire 392
retardancy standards for industrial applications.¹⁶ 393

The comparison between neat PA6 matrix and PA6/SHNTs 394
nanocomposite shows that CO emission is stronger for the 395
nanocomposite with a first peak at lower time. Besides, this 396
tendency is confirmed for PA6/1HNTs (Figure 3c) with its CO 397
curve just inserted between the two other CO curves. This 398
suggests better char formation in the presence of HNTs. This 399
easier char formation could be related to the lower thermal 400
stability for the composite shown by TGA and PCFC, which 401
indicate that the release of water from the clays leads to 402
hydrolysis of PA6 polymer chains. Since the emission of particles 403
is significantly lower for neat PA6, it shows that the char is more 404
unstable with the unfilled polymer, and burns more easily. 405

We can thus surmise that the HNTs modify the thermal 406
behavior of the PA6/HNTs nanocomposite during its 407
incineration and that the more HNTs incorporated in PA6, the 408
more the phenomenon is accentuated. In fact, these nanoclays 409
enhance PA6's ability to form a protective char layer, and 410
reinforce it via a cohesive char/HNTs layer. To sum up, through 411
a two-step mechanism as suggested by analysis of the time 412
tracking, this char/HNTs layer gradually forms, acts as a barrier, 413
cracks, oxidizes and ends up entirely inorganic. 414

5.2. Fate of HNTs: Aggregates in Aerosol and Residues. 415
The imagery results reveal the presence of mineral nano-objects 416
in both the combustion aerosol and the combustion residues as 417
aggregates and as prismatic (pseudotubular) structures which 418
could result from partial distortion of the tubular structure. 419

Thus, HNTs are not destroyed during the incineration of 420
PA6/HNTs nanocomposites, but seem to be transformed into 421
other mineral structures (named HNTs*). Only qualitative 422
considerations can be discussed here. 423

At high temperatures (beyond 1000 °C), the tubular 424
morphology tends to distort and then halloysite transforms 425
into new crystalline or amorphous structures such as gamma- 426
alumina, cristobalite, and mullite.⁴¹⁻⁴³ Actually, it is established 427
that thermal decomposition of HNTs occurs in three steps: 428
dehydration (loss of H_2O from ~200 °C), dehydroxylation (loss 429
of OH from ~500 to 900 °C) and a mullite-like phase formation 430
(from 1200 to 1400 °C). The distortion of the tubular structure 431
begins from 1000 °C and fusion up to 1400 °C.⁴¹⁻⁴³ Considering 432
the high temperatures reached in the furnace (at least 850 °C and 433
more in the presence of a flame), the HNTs undergo the 434
aforementioned thermal transitions during the incineration of 435
PA6/HNTs. Thus, the presence of mineral aggregates identified 436
as pseudo-HNTs with transformed mineral structures (HNTs*) 437
could be explained by the thermal process occurred during the 438
HNTs' stay in the furnace, and the aggregated state could also be 439
explained by a sintering process occurring during the stay above 440
850 °C. Nevertheless, the temperature is not high enough to 441
ensure the crystallization of mullite. 442

Finally, regarding the behavior of multilayered silicates, it can 443
be suggested that for the incineration of other PA6/silicate 444
nanocomposites, mineral nano-objects could be found both in 445
the aerosol downstream of the postcombustion chamber and in 446
residues, but possibly transformed into other mineral structures, 447
taking into account the temperature of the incinerator and the 448
residence time. This should be confirmed by prospective 449
additional incineration tests on other nanocomposites. 450

451 **5.3. Concerns about Incineration of Waste Containing**
 452 **Nanomaterials.** A nanomaterial can be defined as any
 453 intentionally manufactured material, containing particles, in an
 454 unbound state or as an aggregate or as an agglomerate and where,
 455 for 50% or more of the particles in the number size distribution,
 456 one or more external dimensions is in the size range 1–100 nm,
 457 according to the European Commission article 18(5) of
 458 Regulation 1169/2011.⁴⁴ Their potential releases in the
 459 environment during their life cycle and their subsequent impacts
 460 on health have been an increasing concern for many years. Toxic
 461 effects of different types of nanomaterials have been studied and
 462 demonstrated.^{45,46} Nevertheless, the data are incomplete and
 463 detailed studies are required.
 464 The aim of the present study was to provide an insight into
 465 hazards regarding the incineration of waste containing nanoma-
 466 terials from nanocomposites. Therefore, lab-scale tests were
 467 performed to investigate the release of nano-objects downstream
 468 of the postcombustion chamber and the presence of nano-
 469 objects in slag residues. Nano-objects from nanocomposites were
 470 found in the combustion aerosol and in residues. This leads to
 471 the conclusion that both flue gas and slag treatments would be
 472 affected by concerns about nanomaterial incineration and the
 473 potential precautions to be taken.

478 ■ AUTHOR INFORMATION

479 Corresponding Authors

480 *(J.-M.L.-C.) E-mail: Jose-Marie.Lopez-Cuesta@mines-ales.fr.

481 *(O.L..B.) E-mail: Olivier.LE-BIHAN@ineris.fr.

482 Notes

483 The authors declare no competing financial interest.

484 ■ ACKNOWLEDGMENTS

485 Financial support for this work was provided by ADEME,
 486 INERIS, and LNE. We are grateful to their colleagues from
 487 INERIS, Trédi (Séché Environnement), C2MA (Centre des
 488 matériaux des Mines d'Alès), IMN (Institut des Matériaux de
 489 Nantes) for their advice and technical support. Special thanks go
 490 to Anthony Chesnaud (Centre des Matériaux de Mines
 491 ParisTech) and Dr Gwenn Le Saout (Centre des Matériaux
 492 des Mines d'Alès) for their respective contributions to TEM
 493 imagery and X-ray diffraction.

494 ■ REFERENCES

495 (1) Gao, F. Clay/polymer composites: The story. *Mater. Today*. **2004**,
 496 *7* (11), 1–72 DOI: 10.1016/S1369-7021(04)00509-7.
 497 (2) Jang, B. N.; Wilkie, C. A. The effect of clay on the thermal
 498 degradation of polyamide 6 in polyamide 6/clay nanocomposites.
 499 *Polymer*. **2005**, *46* (10), 3264–3274 DOI: 10.1016/j.poly-
 500 mer.2005.02.078.
 501 (3) Giannelis, E. P. Polymer-Layered Silicate Nanocomposites:
 502 Synthesis, properties and applications. *Appl. Organometal. Chem.*
 503 **1998**, *12*, 675–680 DOI: 10.1002/(SICI)10990739(199810/11)
 504 12:10/113.0.CO;2-V.
 505 (4) Cho, J. W.; Paul, D. R. Nylon 6 nanocomposites by melt
 506 compounding. *Polymer*. **2001**, *42* (3), 1083–1094 DOI: 10.1016/
 507 S0032-3861(00)00380-3.
 508 (5) Roes, L.; Patel, M. K.; Worrell, E.; Ludwig, C. Preliminary
 509 evaluation of risks related to waste incineration of polymer nano-

composites. *Sci. Total Environ.* **2012**, 417–418 76–86 DOI: 10.1016/
 j.scitotenv.2011.12.030. 510

(6) Walser, T.; Limbach, L.-K.; Brogioli, R.; Erismann, E.; Flamigni, L.;
 Günther, D.; Stark, W.-J. Persistence of engineered nanoparticles in a
 municipal solid-waste incineration plant. *Nat. Nanotechnol. Lett.* **2012**, *7*,
 520–524 DOI: 10.1038/NNANO.2012.64. 511

(7) Mueller, N. C.; Buha, J.; Wang, J.; Ulrich, A.; Nowack, B. Modeling
 the flows of engineered nanomaterials during waste handling. *Environ.*
Sci.: Processes Impacts. **2013**, *15*, 251–259 DOI: 10.1039/
 C2EM30761H. 512

(8) Holder, A. L.; Vejerano, E. P.; Zhou, X.; Marr, L. C. Nanomaterial
 disposal by incineration. *Environ. Sci. Process Impacts.* **2013**, *15*, 1652–
 1664 DOI: 10.1039/C3EM00224A. 513

(9) Vejerano, E. P.; Holder, A. L.; Marr, L. C. Emissions of Polycyclic
 Aromatic Hydrocarbons, Polychlorinated Dibenzo-p-Dioxins, and
 Dibenzofurans from Incineration of Nanomaterials. *Environ. Sci.*
Technol. **2013**, *47*, 4866–4874 DOI: 10.1021/es304895z. 514

(10) Vejerano, E. P.; Leon, E. C.; Holdera, A. L.; Marr, L. C.
 Characterization of particle emissions and fate of nanomaterials during
 incineration. *Environ. Sci.: Nano* **2014**, *1*, 133–143 DOI: 10.1039/
 C3EN00080J. 515

(11) Massari, A.; Beggio, M.; Hreglich, S.; Marin, R.; Zuin, S. Behavior
 of TiO₂ nanoparticles during incineration of solid paint waste: A lab-
 scale test. *Waste Management.* **2014**, DOI: 10.1016/j.was-
 man.2014.05.015. 516

(12) Stahlmecke, B.; Asbach, C.; Todea, A.; Kaminski, H.; Kuhlbusch,
 T. A. J. Investigations on CNT Release from Composite Materials
 During End of Life. In *Handbook of Nanosafety: Measurement, Exposure*
and Toxicology; Elsevier, Eds.; Vogel, U., Savolainen, K, Wu, Q., van
 Tongeren, M., Brower, D., Berges, M. 2014; pp242–255. 517

(13) Fornes, T. D.; Paul, D. R. Modeling properties of nylon 6/clay
 nanocomposites using composite theories. *Polymer* **2003**, *44*, 4993–
 5013 DOI: 10.1016/S0032-3861(03)00471-3. 518

(14) Guo, B.; Zou, Q.; Lei, Y.; Jia, D. Structure and Performance of
 Polyamide 6/Halloysite Nanotubes Nanocomposites. *Polym. J.* **2009**, *41*
 (10), 835–842 DOI: 10.1295/polymj.PJ2009110. 519

(15) Heddicke-Höchstötter, K.; Lim, G. T.; Altstädt, V. Novel
 polyamide nanocomposites based on silicate nanotubes of the mineral
 halloysite. *Compos. Sci. Technol.* **2009**, *69*, 330–334 DOI: 10.1016/
 j.compscitech.2008.10.011. 520

(16) Marney, D. C. O.; Russell, L. J.; Wu, D. Y.; Nguyen, T.; Cramm,
 D.; Rigopoulos, N.; Wright, N.; Greaves, M. The suitability of halloysite
 nanotubes as a fire retardant for nylon 6. *Polym. Degrad. Stab.* **2008**, *93*,
 1971–1978 DOI: 10.1016/j.polymdegradstab.2008.06.018. 521

(17) Liu, M.; Jia, D.; Zhou, C. Recent advance in research on halloysite
 nanotubes-polymer nanocomposite. *Prog. Polym. Sci.* **2014**,
 DOI: 10.1016/j.progpolymsci.2014.04.004. 522

(18) Du, M.; Guo, B.; Jia, D. Newly emerging applications of halloysite
 nanotubes: A review. *Polym. Int.* **2010**, *59*, 574–582 DOI: 10.1002/
 pi.2754. 523

(19) Kamble, R.; Ghag, M.; Gaikawad, S.; Panda, B. K. Halloysite
 nanotubes and applications: A review. *J. Adv. Scient. Res.* **2012**, *3*, 25–29
 DOI: 10.1002/pi.2754. 524

(20) Bouillard, J.; R'mili, B.; Moranviller, D.; Vignes, A.; Le Bihan, O.;
 Ustache, A.; Bomfim, J. A.; Frejafon, E.; Fleury, D. Nanosafety by design:
 Risks from nanocomposite/nanowaste combustion. *J. Nanopart. Res.*
2013, *15*, 15–19 DOI: 10.1007/s11051-013-1519-3. 525

(21) Motzkus, C.; Chivas-Joly, C.; Guillaume, E.; Ducourtieux, S.;
 Saragoza, L.; Lesenechal, D.; Macé, T.; Lopez-Cuesta, J.-M.; Longuet, C.
 Aerosols emitted by the combustion of polymers containing nano-
 particles. *J. Nanopart. Res.* **2012**, *14*, 1–17 DOI: 10.1051/rfm/2012009. 526

(22) Chivas-Joly, C.; Motzkus, C.; Guillaume, E.; Ducourtieux, S.;
 Saragoza, L.; Lesenechal, D.; Lopez-Cuesta, J.-M.; Longuet, C.; Sonnier,
 R.; Minisini, B. Influence of carbon nanotubes on fire behaviour and
 aerosol emitted during combustion of thermoplastics. *Fire Mater.* **2014**,
38, 46–62 DOI: 10.1002/fam.2161. 527

(23) Rhodes, J.; Smith, C.; Stec, A. Characterisation of soot particulates
 from fire retarded and nanocomposite materials, and their toxicological
 528

- 578 impact. *Polym. Degrad. Stab.* **2011**, *96*, 277–284 DOI: 10.1016/
579 j.polymdegradstab.2010.07.002.
- 580 (24) Kashiwagi, T.; Harris, R. H.; Zhang, X.; Briber, R. M.; Cipriano, B.
581 H.; Raghavan, S. R.; Awad, W. H.; Shields, J. R. Flame retardant
582 mechanism of polyamide 6–clay nanocomposite. *Polymer* **2004**, *45*,
583 881–891.
- 584 (25) Lewin, M.; Pearce, E. M.; Levon, K.; Mey-Marom, A.;
585 Zammarano, M. C. A.; Wilkie Jang, B. N. Nanocomposites at elevated
586 temperatures: Migration and structural changes. *Polym. Adv. Technol.*
587 **2006**, *17*, 226–234 DOI: 10.1002/pat.684.
- 588 (26) Walters, R. N.; Lyon, R. E. Molar group contributions to polymer
589 flammability. *J. Appl. Polym. Sci.* **2003**, *87*, 548–563 DOI: 10.1002/
590 app.11466.
- 591 (27) BREF Waste Incineration 2006, Reference document on best
592 available techniques [http://www.ineris.fr/ipcc/sites/default/files/files/
593 wi_bref_0806.pdf](http://www.ineris.fr/ipcc/sites/default/files/files/wi_bref_0806.pdf) (accessed on June 2014).
- 594 (28) Niemelä V., Lamminen E., Laitinen A. A Novel method for
595 particle sampling and size-classified electrical charge measurement at
596 power plant environment. In *11th International Conference on Electro-
597 static Precipitation*, 2009.
- 598 (29) Andersson J., Mamakos A., Giechaskiel B., Carriero M., Martini G.
599 *Particle Measurement Programme (PMP) Heavy-Duty Inter-Laboratory
600 Correlation Exercise (ILCE_HD) Final Report*, GRPE-PMP-25-05. 2010.
- 601 (30) Motzkus, C.; Chivas-Joly, C.; Guillaume, E.; Ducourtieux, S.;
602 Saragoza, L.; Lesenechal, D.; Mace, T.; Lopez-Cuesta, J.-M.; Longuet, C.
603 Aerosols emitted by the combustion of polymers containing nano-
604 particles. *J. Nanopart. Res.* **2012**, *14*, 1–17 DOI: 10.1007/s11051-011-
605 0687-2.
- 606 (31) Tissari, J.; Hytonen, K.; Lyyranen, J.; Jokiniemi, J. A novel field
607 measurement method for determining fine particle and gas emissions
608 from residential wood combustion. *Atmos. Environ.* **2007**, *41*, 8330–
609 8344 DOI: 10.1016/j.atmosenv.2007.06.018.
- 610 (32) Keskinen, J.; Pietarinen, K.; Lehtimäki, M. Electrical low pressure
611 impactor. *J. Aerosol Sci.* **1992**, *23*, 353–360 DOI: 10.1016/0021-
612 8502(92)90004-F.
- 613 (33) Lyyrinen, J.; Jokiniemi, J.; Kauppinen, E. I.; Backman, U.; Vesala,
614 H. Comparison of different dilution methods for measuring diesel
615 particle emissions. *Aerosol Sci. Technol.* **2004**, *38*, 12–23 DOI: 10.1080/
616 02786820490247579.
- 617 (34) Sarvi, A.; Lyyrinen, J.; Jokiniemi, J.; Zevenhoven, R. Particulate
618 emissions from large-scale medium-speed diesel engines: 2. Chemical
619 composition. *Fuel Process. Technol.* **2011**, *92*, 2116–2122 [http://dx.doi.
620 org/10.1016/j.fuproc.2011.06.021](http://dx.doi.org/10.1016/j.fuproc.2011.06.021).
- 621 (35) R'mili, B.; Le Bihan, O.; Dutouquet, C.; Aguerre-Chariol, O.;
622 Frejafon, E. Particle sampling by TEM grid filtration. *Aerosol Sci. Technol.*
623 **2013**, *47* (7), 767–775 DOI: 10.1080/02786826.2013.789478.
- 624 (36) Davis, R. D.; Gilman, J. W.; Vander Hart, D. L. Processing
625 degradation of polyamide 6/montmorillonite clay nanocomposites and
626 clay organic modifier. *Polym. Degrad. Stab.* **2003**, *79*, 111–121
627 DOI: 10.1016/S0141-3910(02)00263-X.
- 628 (37) Vaia, R. A.; Price, G.; Ruth, P. N.; Nguyen, H. T.; Lichtenhan, J.
629 Polymer layered silicate nanocomposites as high performance ablative
630 materials. *Appl. Clay Sci.* **1999**, *15*, 67–92 DOI: 10.1016/S0169-
631 1317(99)00013-7.
- 632 (38) Gilman, J. W.; Kashiwagi, T.; Harris, R. H. Jr.; Lomakin, S. M.;
633 Lichtenhan, J. D.; Bolf, A.; Jones, P. Char enhancing approaches to flame
634 retarding polymers, *Chem. Technol. Polym. Addit.* 1999, Chapter 8,
635 Blackwell Science Inc., Malden, MA, Ak-Malaika, S.; Golovoy, A.;
636 Wilkie, C. A., 135–150.
- 637 (39) Bahramian, A. R.; Kokabi, M.; Famili, M. H. N.; Beheshty, M. H.
638 High temperature ablation of kaolinite layered silicate/phenolic resin/
639 asbestos cloth nanocomposite. *J. Hazard. Mater.* **2008**, *150*, 136–145
640 DOI: 10.1016/j.jhazmat.2007.04.104.
- 641 (40) Lyon, R. E. Pyrolysis kinetics of char forming polymers. *Polym.*
642 *Degrad. Stab.* **1998**, *61*, 201–210 DOI: 10.1016/S0141-3910(97)
643 00125-0.
- 644 (41) Yuan, P.; Tan, D.; Annabi-Bergaya, F.; Yan, W.; Fan, M.; Liu, D.;
645 He, H. Changes in structure, morphology, porosity, and surface activity
of mesoporous halloysite nanotubes under heating. *Clays Clay Miner.* **2012**, *60*, 561–573 DOI: 10.1346/CCMN.2012.0600602.
- (42) Cheng, H.; Frost, R.; Yang, J.; Liu, Q.; He, J. Infrared and infrared
emission spectroscopic study of typical Chinese kaolinite and halloysite.
Spectrochim. Acta **2010**, *77* (Part A), 1014–1020 DOI: 10.1016/
j.saa.2010.08.039.
- (43) Smith, M. E.; Neal, G.; Trigg, B. M.; Drennan, J. Structural
characterization of the thermal transformation of halloysite by solid state
NMR. *Appl. Magn. Reson.* **1993**, *4*, 157–170 DOI: 10.1007/
BF03162561.
- (44) Potocnick J. European Commission Recommendation on the
definition of nanomaterial, 2011/696/EU, 2011.
- (45) Wang, Q.; Yang, Z.; Yanga, Y.; Long, C.; Li, H. A bibliometric
analysis of research on the risk of engineering nanomaterials during
1999–2012. *Sci. Total Environ.* **2014**, *473–474*, 483–489; DOI: [http://
dx.doi.org/10.1016/j.scitotenv.2013.12.066](http://dx.doi.org/10.1016/j.scitotenv.2013.12.066).
- (46) Kühnel, D.; Nickel, C. The OECD expert meeting on
ecotoxicology and environmental fate—Towards the development of
improved OECD guidelines for the testing of nanomaterials. *Sci. Total
Environ.* **2014**, *472*, 347–353 [http://dx.doi.org/10.1016/j.scitotenv.
2013.11.055](http://dx.doi.org/10.1016/j.scitotenv.2013.11.055).